International Journal of Computational Intelligence Systems (2023) 16:36
https://doi.org/10.1007/s44196-023-00209-6

RESEARCH ARTICLE

Tracking Control Based on GPS Intelligent Buoy System for an Autonomous Underwater Vehicles Under Measurement Noise and Measurement Delay

Qiang Liu[1,2] · **Muguo Li**[2]

Received: 22 December 2022 / Accepted: 26 February 2023

Abstract
This paper deals with the real-time tracking control problem for an autonomous underwater vehicle based on an acoustic-based positioning method, i.e., the so-called GPS intelligent buoy system, which causes inevitable measurement delay. The measurement delay increases the control difficulty and degrades the tracking accuracy. Additionally, the exact modeling for an autonomous underwater vehicle is difficult due to uncertain hydrodynamic parameters. Based on these findings, a model-free control scheme is proposed. In the proposed scheme, the GPS intelligent buoy system provides the position signals without velocity measurements. Considering the measurement noise, a robust exact differentiator is used instead of the traditional numerical differentiation method to obtain the derivatives of position signals, which saves the limited actuator energy of autonomous underwater vehicles. Simulations are performed to verify the validity of the proposed control scheme. The results demonstrate that the proposed control scheme can achieve high timeliness and high tracking accuracy for autonomous underwater vehicles. Compared to the conventional model predictive control, the proposed controller requires 89.7% less average calculation time. In addition, the proposed controller outperforms the conventional proportion-differentiation controller in root-mean-square error by approximately 62.3−80.7%.

Keywords GPS intelligent buoy system · Real-time tracking control · Measurement delay · Measurement noise · Robust exact differentiator

Abbreviations

AUV	Autonomous underwater vehicle
ROV	Remotely operated vehicle
GIB	GPS intelligent buoy
GPS	Global positioning system
DVL	Doppler velocity log
IMU	Inertial measurement unit
PID	Proportion integration differentiation
MPC	Model predictive control
TDE	Time delay estimator
TDC	Time delay controller
RED	Robust exact differentiator
LMI	Linear matrix inequality
RMS	Root mean square
ZOH	Zero order hold

1 Introduction

Autonomous underwater vehicles (AUVs) play an extremely important role in deep sea tasks [1], e.g., enemy target tracking [2], sea-bed scanning [3], inspection of deep water oil/gas pipelines, and marine environmental data collection [4]. Currently, underwater robotic vehicles mainly include manned underwater vehicles, tethered unmanned underwater vehicles, i.e., remotely operated vehicles (ROVs), and AUVs [5]. Due to high risk and operational cost, manned underwater vehicles are not a good choice for deep sea tasks. ROVs and AUVs are the two major categories of unmanned underwater vehicles and have much lower operational costs and

✉ Qiang Liu
liuqiang1949@mail.dlut.edu.cn

Muguo Li
lmguo@dlut.edu.cn

[1] Faculty of Electronic Information and Electrical Engineering, Dalian University of Technology, Dalian 116024, Liaoning Province, People's Republic of China

[2] State Key Laboratory of Coastal and Offshore Engineering, Dalian University of Technology, Dalian 116024, Liaoning Province, People's Republic of China

Published online: 18 March 2023

risks than the manned underwater vehicles. An ROV is usually controlled by a surface control center and is subject to the communication delay between the surface control center and ROV. This communication delay results in degradation of tracking performance in deep sea missions. Compared to ROVs, AUVs can autonomously collect data and independently complete predefined tasks. In other words, the control center is located in the AUV. AUVs can also reduce operational costs. However, the positioning for AUV is not convenient as for other devices on land. It is well known that the penetration of electromagnetic signals is poor below the sea surface, so the global positioning system (GPS) is not available for AUV positioning [6]. To solve the AUV positioning problem, a GPS intelligent buoy (GIB) has been used in commercial applications as an acoustic positioning system [7]. Nevertheless, the GIB system has the problem of time-varying communication delay between the AUV and buoys due to the finite speed of sound propagation in water. This indicates that the measurement signals cannot be provided to the controller in a timely manner. The corresponding measurement delay will lead to an undesirable effect on tracking performance of an AUV. In addition, due to the uncertain hydrodynamic parameters, the exact AUV system model is poorly known, which is commonly encountered in practice. These problems make it difficult to drive an AUV precisely to a desired target point in a demanding marine environment.

Deep learning has proven its capabilities in numerous fields including medical recommender systems, object detection, and path planning (e.g., tracking target points). Spurred by deep learning's state-of-the-art capabilities, researchers have already extended artificial intelligence-based techniques into the field of AUV underwater positioning and path planning. For example, [8] suggests a hybrid pipeline, where a deep learning scheme generates low-frequency position information to correct the error accumulation of the navigation system. Then, the x^2 rule determines if the Doppler velocity log (DVL) measurement fails, and an adaptive filter, exploiting the variational Bayesian method, estimates the navigation information. However, although this method is interesting, it relies on GPS data and thus is constrained to surface and low submersing platforms. In [9], the authors utilize a Recurrent Neural Network to predict the AUV's relative horizontal velocities by exploiting data from an Inertial Measurement Unit (IMU), pressure sensor, and control inputs. The RNN network is trained on experimental data with a DVL providing ground truth velocities. Despite this method posing a promising solution for deep learning-based AUV localization, it suffers from substantial errors in the order of hundreds of meters, requiring further research to improve it. Extending the vehicle's localization architecture to AUVs has also been proposed, with [10] extracting features from sonar imagery using a Convolution Neural Network. Although this is a theoretically sound solution, the paper is constrained on the feature matching performance rather than the AUV's trajectory accuracy. In [11], the authors develop a reinforcement learning-based algorithm that solely employs the information measured by the AUV's onboard sensors. Moreover, in this method, the reward function considers different factors substantially affecting the AUV's navigation control accuracy. The experiments reveal that the RL-based technique responds well to disturbances, but no trajectory is presented to evaluate the complete performance of this method. A more sophisticated solution is presented in [12] that considers AUV path planning combining deep learning and reinforcement learning. This promising solution has not yet been evaluated in synthetic or real experiments. Although artificial intelligence-based solutions have been explored, currently, they do not pose a complete off-the-shelf and practical solution as substantial research must be undertaken.

Extensive research has been carried out on the design of tracking controllers for AUVs to address hydrodynamic parameter uncertainties. It is well known that the classical proportion–integration–differentiation (PID) technology has been used in the automatic systems including vehicle control. Considering the parameter uncertainties, Jalving [13] designed three autopilots for steering, diving, and speed control of an AUV based on PID technologies, where the control system was robust and stable for the autopilots. Modern controllers have been developed to cope with the system uncertainties for AUVs. Considering an uncertain model including certain unstructured disturbances, a traditional back-stepping method combined with robust adaptive technologies [14] was proposed for an AUV to address the so-called matching condition problem [15]. Repoulias et al. [16] designed a closed-loop controller to address tracking errors due to uncertain model parameters and external disturbances. Liang et al. [17] suggested a spatial path following controller for an underactuated AUV, where a nonlinear damping term was introduced to offset the influence of dynamic uncertainties and disturbances. In [18], a controller was proposed by combining a back-stepping technique and adaptive dynamical sliding mode control method. The designed controller resolved the environmental disturbances and systematic parametric uncertainties well. Utilizing a back-stepping and sliding mode control technique, a hierarchical robust nonlinear controller was presented for the trajectory tracking of an AUV subject to uncertainties [19]. Specifically, the uncertainties include current disturbances, unmodelled dynamics, and parameter variations. Liang et al. [20] exploited the combination of back-stepping control and sliding mode control to acquire robustness against systematic uncertainties and external disturbances. In the framework of adaptive control, Li et al. [21] developed a novel robust adaptive tracking controller for an AUV subject to unknown dynamic parameters. Wang et al. [22] established an appropriate error dynamics model for an AUV in the presence of parameter uncertainties and

disturbances. The presented adaptive-robust control scheme successfully achieved path following. In [23], a neural adaptive-robust prescribed performance controller was proposed. The proposed controller guaranteed robust stability against unmodelled dynamics and external disturbances. Peng et al. [24] introduced an extended state observer to estimate the extended state composed of unknown internal dynamics and external disturbances. In a previous paper [25], the authors combined neural networks and adaptive control techniques, and obtained good robustness for path following. Nevertheless, most of these modern controllers [14–25] require full or partial knowledge of hydrodynamics and disturbances to be known. Yan et al. [26] described a double closed-loop trajectory tracking method for an AUV based on model predictive control (MPC). In this method, system uncertainty is compensated by a receding horizon implementation. However, the MPC method incurs considerable computational complexity and energy consumption. In practical deep sea tasks, the AUV's energy is usually limited. Thus, the current MPC strategy is not an optimum solution for AUV tasks. For robustness against hydrodynamic uncertainties and external disturbances, time-delay estimator (TDE) has been adopted. Compared to the controllers [14–26], TDE has the advantage of computational simplicity. The main idea of TDE is that assuming the system dynamics are given in the form of piecewise or continuous functions, the variation in the dynamics over a very short period can be negligible; thus, the current value of the dynamics can be estimated circuitously using the past system state and input information. Utilizing TDE techniques, some time-delay controllers (TDCs) have been proposed to solve the case of system uncertainties and disturbances. Kumar et al. [27] first introduced the TDE technique into AUV control. The designed TDC used the feedback of delayed accelerations and control inputs to approximately cancel the unknown dynamics of the plant and unexpected disturbances. Kim et al. [28] developed an integral sliding-mode controller to supplement a conventional TDC and decrease the TDE error due to slow data acquisition rate when a DVL navigation system is in operation. Cho et al. [29] suggested a robust controller combining a back-stepping approach and TDE for the trajectory tracking of an AUV subject to highly nonlinear dynamics and external disturbances. Mahmood et al. [30] employed a TDC and nonlinear disturbance observer simultaneously to address parametric uncertainties and thereby provided an attractive model-free structure. Nevertheless, these controllers [27–30] do not consider the time-varying measurement delay problem. In addition, the implementation of TDE requires prior information of the derivative of the system state, i.e., the acceleration is known in advance. The acceleration is generally acquired by a traditional numerical differentiation method [27–30], i.e., the differential of the velocity signal or twice the differential of the position signal. However, measurement position signals are inevitably affected by noise due to the complex operational conditions and the surrounding environment. Thus, the traditional numerical differentiation method introduces nonnegligible measurement noise into the acceleration [31]. This results in the deterioration of tracking performance. Different from the numerical differentiation method, a state-derivatives estimation technique was adopted in a time-delayed adaptive-robust control strategy [32]. The state-derivatives estimation procedure itself had the ability to suppress the measurement noise. The presented time-delayed adaptive-robust control provided an appealing solution to the existing issues of TDE-based controllers and conventional ARCs. However, the controller assumes that the feedback position signals were timely regardless of potential delay issue.

Due to complex marine environment, positioning is particularly challenging for AUV. Thus, tackling the positioning problem for AUV navigation is a current research focus [33–35]. With accurate positioning, an AUV can accomplish deep sea tracking tasks well. Given that a GPS navigation system for an AUV is not available due to the high attenuation rate of GPS signals in the deep sea, the alternative solutions are inertial navigation and acoustic navigation systems. In an inertial navigation system, onboard inertial sensors mainly include accelerometers, gyroscopes, magnetometers, DVLs, and depth sensors [36]. The AUV's relative position and velocity can be estimated by different sensor data combined with appropriate filter algorithms. Nevertheless, these onboard sensor measurements are sensitive to physical conditions and lead to significant error accumulation in practice. In addition, the complex environment and high water pressure in the deep sea make the mechanical design of sensors embedded in an AUV difficult. Compared to inertial navigation, acoustic navigation has better accuracy but also a higher cost [37]. With the aid of multiple acoustic transponders, the acoustic navigation system uses the time of flight concept to estimate the position of an AUV. One of the popular acoustic navigation systems is a GIB that has been used commercially for AUV positioning. Since position estimates are available only at the central station, a GIB system is naturally suited for AUV tracking applications [38]. However, the communication delay between the AUV and buoys hinders the design of the tracking controller. There is a little literature focusing on communication delay in the field of AUV control. A region tracking controller was proposed to navigate an AUV within a specific region with known constant input delay, but robustness to model-based uncertainties and external disturbances is not addressed [39]. Yan et al. [40] presented a fast terminal sliding mode observer to estimate the velocity of an AUV. The designed observer performance was not affected directly by the communication delays between the AUV and buoys. In the field of aircraft control, [41] presented a trajectory tracking control scheme for unstable aircraft with delayed measurement.

In the presented scheme, a Lyapunov–Krasovskii functional and linear matrix inequality (LMI) technique are used to obtain a delay-dependent sufficient criterion. In the field of ROV control [42, 43], developed tracking controllers to address the communication delay between the surface control center and ROV. Nevertheless, these controller assumed that the velocity signal was measurable, while GIB systems only provided position signals for AUV.

Inspired by the discussions above, we consider the combined nuisance factors of uncertain hydrodynamic parameters along with measurement delay. In addition, energy efficiency and timeliness are important criteria for designing AUV tracking controllers. These findings motivate us to favor controllers that are computationally easy to implement and suitable for real-time tracking control. In this study, a target points tracking controller based on underwater positioning system is proposed for an AUV with consideration of uncertain hydrodynamic parameters, time-varying measurement delay, and measurement noise. The proposed controller could achieve the target points tracking tasks with less energy consumption in a limited time, and obtain appealing position tracking accuracy performance. The main contributions of our work can be summarized as five aspects:

1. We propose a GIB-based model-free controller that can efficiently drive an AUV to arrive at a desired target point under hydrodynamic parameter uncertainties, measurement noise, and an allowable time-varying measurement delay. Note that the presented control law does not require the knowledge of the bounds on uncertainties, which is the norm for practical applications.
2. We analyze system stability for the proposed controller and present a delay-dependent stability criterion, where the allowable upper bound of measurement delay can be calculated.
3. We introduce a robust exact differentiator (RED) into the presented control law to reduce the effect of measurement noise on the position tracking performance. Compared to the traditional numerical differentiation method, the RED is effective improving the position accuracy for target points.
4. We utilize RED to obtain the derivatives of position signals with measurement noise. The control input is not significantly increased thus reducing the energy consumption of AUV.
5. We challenge our proposed AUV target point tracking method in several synthetic scenarios. In the presence of measurement noise, measurement delay, and uncertain hydrodynamics, the suggested control law attains better position control precision than the conventional PD controller. Compared to the advanced control strategy, i.e., MPC controller, our controller affords more appealing computational complexity, i.e., high timeliness.

The remainder of this article is organized into four sections. Section 2 introduces the mathematical model of the AUV and the GIB system. Section 3 describes the presented control law and RED. Section 4 presents the simulation results that illustrate the performance of the proposed controller, and Sect. 5 concludes the work.

2 Modeling and Underwater Positioning

2.1 Mathematical Model of an AUV

The mathematical model includes kinematics and hydrodynamics. To describe the motion of an AUV, an inertial coordinate frame $\{I\}$ and body-fixed coordinate frame $\{B\}$ are used, as shown in Fig. 1. Specifically, the position and attitude, velocity, and acceleration are represented by frames $\{I\}$ and $\{B\}$, respectively. In particular, Fig. 2 shows the motions represented simultaneously by frame $\{I\}$ and frame $\{B\}$ in the horizontal plane.

For frame $\{I\}$, the six degree-of-freedom (DOF) AUV kinematic equation is defined as follows [1]:

$$\dot{\boldsymbol{\eta}} = \boldsymbol{J}(\boldsymbol{\eta})\boldsymbol{v} \tag{1}$$

Likewise, the 6-DOF AUV hydrodynamic equation is described in frame $\{B\}$ as follows [1]:

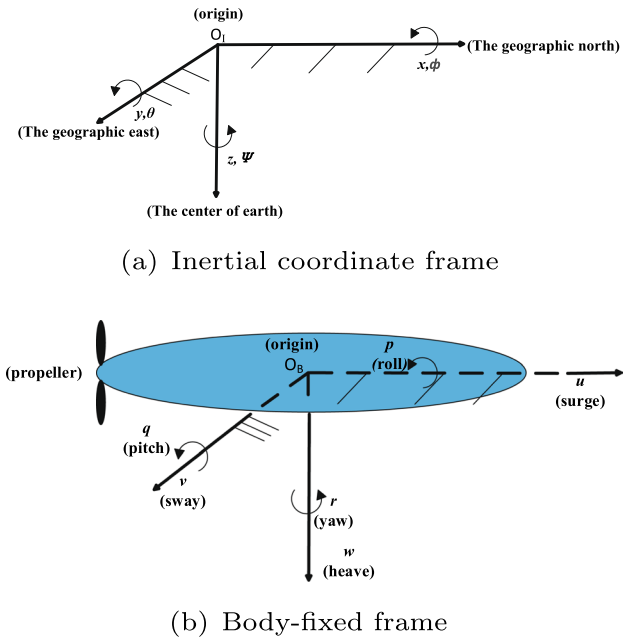

Fig. 1 Tracking reference frames

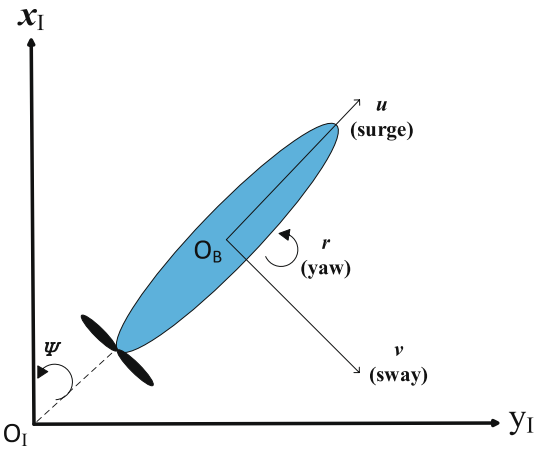

Fig. 2 AUV motions represented by the frames $\{I\}$ and $\{B\}$ in the horizontal plane

$$\boldsymbol{M\dot{v} + C(v)v + D(v)v + g(\eta) = \tau} \tag{2}$$

In Eq. (1), $\boldsymbol{\eta} = [x\ y\ z\ \phi\ \theta\ \psi]^T$ is the position and attitude vector of the AUV in frame $\{I\}$. Specifically, x, y, and z denote the positions of AUV in surge, sway, and heave, respectively. ϕ, θ, and ψ are the attitude (i.e., Euler angles) in roll, pitch and yaw, respectively. The non-singular $\boldsymbol{J(\eta)}$ is a rotation matrix from the $\{B\}$ frame to the $\{I\}$ frame. $\boldsymbol{v} = [u\ v\ w\ p\ q\ r]^T$ denotes the velocity vector of the AUV in frame $\{B\}$, $[u\ v\ w]^T$ represents the linear velocities and $[\,p\ q\ r]^T$ represents the angular velocities.

In Eq. (2), $\boldsymbol{M = M_{RB} + M_A}$ is the positive definite inertia matrix, and $\boldsymbol{M_{RB}}$ and $\boldsymbol{M_A}$ represent the rigid body mass matrix and the added mass matrix, respectively. $\boldsymbol{C(v)}$ is the Coriolis and the centripetal terms matrix of the rigid body ($\boldsymbol{C_{RB}}$) with added mass ($\boldsymbol{C_A}$). $\boldsymbol{D(v)}$ is the damping matrix including the linear and quadratic drag terms. The vector $\boldsymbol{g(\eta)}$ represents the restoring forces and moments. $\boldsymbol{\tau}$ is control input consisting of forces and moments.

From Eqs. (1) and (2), we can rewrite the AUV dynamic system as follows:

$$\boldsymbol{M_\eta\ddot{\eta} + C_\eta(v,\eta)\dot{\eta} + D_\eta(v,\eta)\dot{\eta} + g_\eta(\eta) = \tau_\eta} \tag{3}$$

where $\boldsymbol{M_\eta = J^{-T}MJ^{-1}}$, $\boldsymbol{C_\eta(v,\eta) = J^{-T}[C - MJ^{-1}\dot{J}]J^{-1}}$, $\boldsymbol{D_\eta(v,\eta) = J^{-T}DJ^{-1}}$, $\boldsymbol{g_\eta(\eta) = J^{-T}g(\eta)}$, and $\boldsymbol{\tau_\eta = J^{-T}\tau}$. The equation (3) is intended to facilitate the analysis of system stability later.

The important properties are expressed as follows [44, 45]:

- The center of mass of the vehicle is the origin O_B of frame $\{B\}$.
- The inertia matrix $\boldsymbol{M_\eta}$ is bounded and symmetric positive definite.
- The damping matrix $\boldsymbol{D_\eta(v,\eta)}$ is positive definite.
- Matrix $\boldsymbol{M_\eta - 2C_\eta(v,\eta)}$ is skew-symmetric.
- During the controller design, all AUV model parameters are unknown and hydrodynamic parameters are uncertain.

Most open-frame AUVs are inherently stable with respect to pitch and roll. Therefore, we neglect the pitch and roll motions in our work and obtain the 4-DOF hydrodynamics of AUV:

$$m_u\dot{u} - m_v vr + k_u u + k_{u|u|}|u|u = F_u \tag{4}$$

$$m_v\dot{v} + m_u ur + k_v v + k_{v|v|}|v|v = F_v \tag{5}$$

$$m_w\dot{w} + k_w w + k_{w|w|}|w|w = F_w + W(t) \tag{6}$$

$$I_r\dot{r} + (m_v - m_u)uv + k_r r + k_{r|r|}|r| = T_r \tag{7}$$

where m_u, m_v, and m_w denote the masses in surge, sway, and heave, respectively. $\boldsymbol{I}_r$ represents the moment of inertia in yaw. $k_u/\ k_{u|u|}$, $k_v/\ k_{v|v|}$, and $k_w/\ k_{w|w|}$ and $k_r/\ k_{r|r|}$ are the linear/quadratic damping coefficients. F_u, F_v, and F_w are the input forces in surge, sway, and heave, respectively. $\boldsymbol{T}_r$ describes the external turning moment in yaw. $W(t)$ represents restoring force in heave.

In addition, the yaw angle is sufficiently controlled by the autopilot installed on the open-frame AUV. Thus, we assume that yaw angle is constant, i.e., $\psi(t) = \psi_c$, and simplify the AUV model to 3-DOF. Hence, we obtain [46]:

$$\boldsymbol{M} = \begin{bmatrix} m_u & 0 & 0 \\ 0 & m_v & 0 \\ 0 & 0 & m_w \end{bmatrix} \tag{8}$$

$$\boldsymbol{D(v(t))} = \begin{bmatrix} k_u + k_{u|u|}|u(t)| & 0 & 0 \\ 0 & k_v + k_{v|v|}|v(t)| & 0 \\ 0 & 0 & k_w + k_{w|w|}|w(t)| \end{bmatrix} \tag{9}$$

$$\boldsymbol{C(v(t))} = \boldsymbol{O}_{3\times 3} \tag{10}$$

$$\boldsymbol{g(\eta(t))} = [0 \quad 0 \quad -W(t)]^T \tag{11}$$

$$\boldsymbol{\tau}(t) = [F_u(t) \quad F_v(t) \quad F_w(t)]^T \tag{12}$$

$$\boldsymbol{J}(\boldsymbol{\eta}(t)) = \begin{bmatrix} \cos(\psi_c) & -\sin(\psi_c) & 0 \\ \sin(\psi_c) & \cos(\psi_c) & 0 \\ 0 & 1 & 0 \end{bmatrix} \tag{13}$$

2.2 Underwater Positioning

An acoustic positioning-based GIB system (see Fig. 3 is adopted [5], which can provide the position signals to the AUV controller. In the GIB system, buoys whose clocks are synchronized with those of the AUV are deployed over the surface and periodically emit acoustic signals. The period is T_G. Then, the control center of the AUV obtains the times of arrival of these acoustic signals to calculate an estimated position of the AUV. There is a time-varying communication delay from the buoys to the AUV. In general, a longer distance between the AUV and buoys corresponds to greater communication delay. In addition, the calculated time is considered. Thus, the total measurement delay $d(t)$ includes the communication time $d_{co}(t)$ and the calculated time $d_{ca}(t)$, i.e., $d(t) = d_{co}(t) + d_{ca}(t)$. Here, an assumption is made as follows:

Assumption 1 The measurement delay $d(t)$ and its derivative $\dot{d}(t)$ are lower and upper bounded, i.e., satisfying the limitation [41]

$$d(t) \in [d_{\min}, d_{\max}], \quad \dot{d}(t) \in [a_{\min}, a_{\max}] \tag{14}$$

where $0 \le d_{\min} \le d_{\max}$ and $a_{\min} \le a_{\max} \le 1$. $d_{\min}$ and $d_{\max}$ denote positive scalars representing the minimum and maximum delay, respectively. Likewise, $a_{\min}$ and $a_{\max}$ are the minimum derivative and maximum derivative, respectively.

Remark 1 The traditional GIB system [38] and the extended GIB system [5] both encounter the problem of measurement delay. Thus, our study does not lose generality.

Remark 2 It is worth noting that we use zero-order hold (ZOH) to bridge the GIB system and the continuous-time control system. Thus, the measurement position signal is continuous for AUV control system.

3 Control Synthesis

In this section, we present an AUV tracking control system that can operate under uncertain hydrodynamic parameters and time-varying measurement delays. The proposed scheme is shown in Fig. 4. The presented controller with a time-varying measurement delay drives the AUV system to arrive at the target point. Because the GIB system only provides position signals without velocity signals, the RED is used instead of the traditional numerical differentiation method to obtain the derivative of the position signal, which saves the AUV's limited energy. Table 1 describes the main symbols used in this article.

3.1 Control Law with Time-Varying Measurement Delay

In this subsection, the control law with time-varying measurement delay is presented for AUV target points tracking.

Due to uncertain hydrodynamic parameters, an exact AUV model is generally impossible to obtain. Thus, we use the model-free control method and obtain the following control law

$$\begin{aligned} \boldsymbol{\tau}(t) = \boldsymbol{J}^T[\boldsymbol{K}_P(\boldsymbol{\eta}_d - \boldsymbol{\eta}(t - d(t))) \\ + \boldsymbol{K}_D\dot{\boldsymbol{\eta}}(t - d(t))] + \boldsymbol{g}(\eta) \end{aligned} \tag{15}$$

where $\boldsymbol{K}_P$ and $\boldsymbol{K}_D$ denote the proportional and derivative symmetric gain matrices, respectively, and $\boldsymbol{J}$ is the constant rotation matrix.

Remark 3 The presented control law uses the derivative of the position signal. In our study, the measurement noise is considered. In order to obtain the derivative of the position signal, the traditional numerical differentiation method will magnify the amplitude of measurement noise, which results in a significant control input. Therefore, it is necessary to find an alternative method to obtain the derivative of the position signal for real-time control system.

3.2 System Stability Analysis

The control objective is that the tracking error $\boldsymbol{e} = \boldsymbol{\eta}(t) - \boldsymbol{\eta}_d$ asymptotically converges to zero using proposed control law. The following Lemmas are introduced to analyze the stability of the proposed controller.

Lemma 1 ([47]) *Consider a given positive definite matrix* $\boldsymbol{R} \succ 0$. *Then, for any continuous function* ω *in* $[a, b] \to \mathbb{R}^n$, *the following inequality holds*:

$$\begin{aligned} \ell_R(\omega) \ge \frac{1}{b-a}\left(\int_a^b \omega(\zeta)\,d\zeta\right)^T \boldsymbol{R}\left(\int_a^b \omega(\zeta)\,d\zeta\right) \\ + \frac{3}{b-a}\Omega^T\boldsymbol{R}\Omega \end{aligned} \tag{16}$$

where $\ell_R(\omega) = \int_a^b \omega^T(\zeta)\boldsymbol{R}\omega(\zeta)\,d\zeta$ *and* $\Omega = \int_a^b \omega(s)\,ds - \frac{2}{b-a}\int_a^b\int_a^s \omega(\sigma)d\sigma ds$.

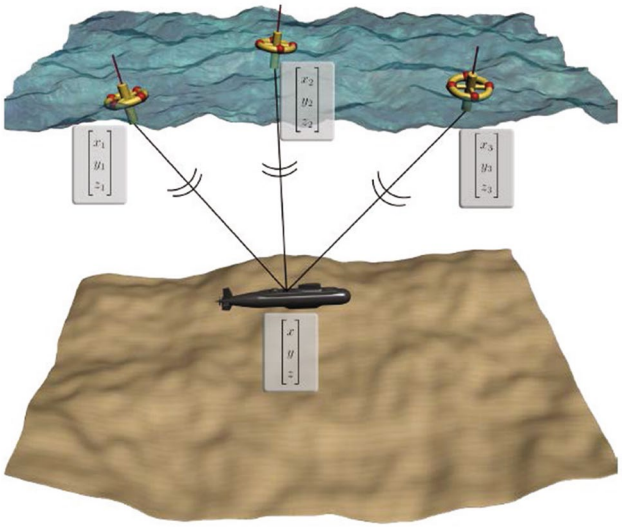

Fig. 3 The GIB system [5]

Lemma 2 ([48]) *For given positive integers n, and m, a scalar α in the interval* (0, 1), *a given* $n \times n$ *matrix* $\boldsymbol{R} \succ 0$, *two matrices* W_1 *and* W_2 *in* $\mathbb{R}^{n\times m}$, *a vector* ξ *in* $\mathbb{R}^m$, *and a defined function* $\Theta(\alpha, \boldsymbol{R}) = \frac{1}{\alpha}\xi^T {W_1}^T \boldsymbol{R} W_1 \xi + \frac{1}{1-\alpha}\xi^T {W_2}^T \boldsymbol{R} W_2 \xi$. *Then, if there exists a matrix* $\boldsymbol{X}$ *in* $\mathbb{R}^{n\times n}$ *such that* $\begin{bmatrix} \boldsymbol{R} & \boldsymbol{X} \\ * & \boldsymbol{R} \end{bmatrix} \succ 0$, *the following inequality holds:*

$$\min_{\alpha\in(0,1)} \Theta(\alpha, \boldsymbol{R}) \geq \begin{bmatrix} W_1\xi \\ W_2\xi \end{bmatrix}^T \begin{bmatrix} \boldsymbol{R} & \boldsymbol{X} \\ * & \boldsymbol{R} \end{bmatrix} \begin{bmatrix} W_1\xi \\ W_2\xi \end{bmatrix} \tag{17}$$

Next, the stability theorem using the proposed control law is provided as follows:

Theorem 1 *Assume that there exist* 3×3 *positive definite matrices* $\boldsymbol{R}, \boldsymbol{A}, \boldsymbol{B}, \boldsymbol{E}, \boldsymbol{F}, \boldsymbol{G}$, *matrices* $\boldsymbol{X} \in \mathbb{R}^{3\times3}$, $\boldsymbol{H} \in \mathbb{R}^{27\times3}$, $\boldsymbol{K} \in \mathbb{R}^{27\times3}$, *and* $\Phi_{1,k}(\eta, \dot{\eta}) \in \mathbb{R}^{27\times27}$ *such that the following LMIs are satisfied for* $d(t) = \{d_{\min}, d_{\max}\}$ *and* $\dot{d}(t) = \{a_{\min}, a_{\max}\}$

$$\Phi_1(\eta, \dot{\eta}) = \Phi_{1,k}(\eta, \dot{\eta}) - \frac{1}{d_{\max}}\Gamma^T \Phi_2 \Gamma \prec 0 \tag{18}$$

$$\Phi_2 = \begin{bmatrix} \tilde{\boldsymbol{R}} & \boldsymbol{X} \\ * & \tilde{\boldsymbol{R}} \end{bmatrix} \succ 0 \tag{19}$$

Then the AUV tracking system for a target point under Assumptions 1 is asymptotically stable (i.e., tracking error asymptotically converges to zero) for time-varying measurement delay $d(t)$.

Several notations and the proof for Theorem 1 are presented in the appendix.

Remark 4 We refer to the methods in [43] and [47], which are applicable to our 3-DOF position control based on the GIB positioning system. The structure of the proof is the same as the article of Yan et al. [43]. Here, we are more focused on how to get the derivative of position signal with measurement noise. In the GIB system, velocity signal is not available. If the derivative of the position signal is obtained using traditional numerical differentiation method, it will significantly enlarge the control input and cause a considerable energy consumption of AUV. Thus, we focus on saving the limited energy of AUV. In addition, we also consider the case of uncertain hydrodynamic parameters in the simulations.

3.3 Robust Exact Differentiator for the Presented Control Law

Based on the GIB system, only the measurement of position is available for the proposed controller. In practice, the measurement signal $\boldsymbol{\eta}_m$ contains the measurement noise. Other controllers [27, 29, 30] obtain $\dot{\boldsymbol{\eta}}_m(t)$ directly via numerical differentiation. The traditional numerical differentiation method [31] is given by:

$$\dot{\boldsymbol{\eta}}_m(t) = \frac{\boldsymbol{\eta}_m(t) - \boldsymbol{\eta}_m(t-\lambda)}{\lambda} \tag{20}$$

Here, λ is assumed to be very small. However, due to the extremely small factor λ, the traditional numerical

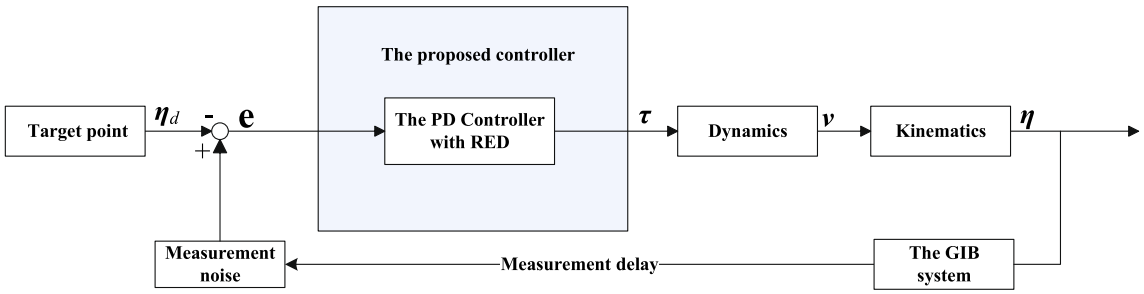

Fig. 4 Schematic diagram of the proposed tracking control

Table 1 The main notations

Symbol	Description	Value
T_G	The period of emitting acoustic signals from buoys	–
$d(t)$	The time-varying measurement delay	–
$\boldsymbol{\eta}$	The real position	–
$\boldsymbol{\eta}_d$	The target point position	–
$\boldsymbol{\eta}_m$	The measurement position from GIB system	–
$\hat{\boldsymbol{\eta}}_m$	The estimated derivative of the position using the RED	–
$\boldsymbol{e}$	The position error	–
$\boldsymbol{K}_P$	The proportional matrix	–
$\boldsymbol{K}_D$	The derivative matrix	–
$\mathbb{R}^{n\times m}$	Set of all real m by n matrices	–
$\boldsymbol{I}$	The identity matrix	–
m	Weight in air	219.8 kg
m_u	Mass in surge	391.5 kg
m_v	Mass in sway	639.6 kg
m_w	Mass in heave	639.6 kg
k_u	Linear damping coefficient in surge	16 kg/s
k_v	Linear damping coefficient in sway	131.8 kg/s
k_w	Linear damping coefficient in heave	65.6 kg/s
$k_{u\|u\|}$	Quadratic damping coefficient in surge	229.4 kg/m
$k_{v\|v\|}$	Quadratic damping coefficient in sway	328.3 kg/m
$k_{w\|w\|}$	Quadratic damping coefficient in heave	296.8 kg/m
$W(t)$	Buoyancy force in heave	−5 N
T_s	MPC sample time	0.1 s
N_p	MPC prediction horizon	10
N_c	MPC control horizon	4
$U_{\max}$	MPC maximum input	400 N
$U_{\min}$	MPC minimum input	−400 N
Q_c	MPC weight on state	$30\boldsymbol{I}_{10\times 10}$
R_c	MPC weight on input	$10\boldsymbol{I}_{12\times 12}$
N_x	Number of state variables	6
N_u	Number of manipulated variables	3

differentiation method introduces non-negligible measurement noise into $\ddot{\boldsymbol{\eta}}_m(t-\lambda)$ and $\dot{\boldsymbol{\eta}}_m(t-d(t))$ in equation (15). To circumvent this problem, a RED [49] is introduced to reduce the measurement noise effects and improve tracking accuracy for target points.

We set $\boldsymbol{\eta}_m(t) = \boldsymbol{\eta}(t) + \boldsymbol{\zeta}(t)$. The signal $\boldsymbol{\eta}_m$ is a measurable locally bounded function defined on [0,∞) and consists of a base signal $\boldsymbol{\eta}(t)$ (i.e., real position) having a derivative with Lipschitz's constant $L_c > 0$ and noise $\boldsymbol{\zeta}(t)$. The noise $\boldsymbol{\zeta}(t)$ is a measurable (Lebesgue) bounded function of time. The practical first-order RED [49] is presented as follows:

$$\begin{cases} \dot{z}_0 = \hat{\boldsymbol{\eta}}_m(t) \\ \dot{z}_0 = -\lambda_1 |z_0 - \boldsymbol{\eta}_m(t)|^{1/2} sign(z_0 - \boldsymbol{\eta}_m(t)) + z_1 \\ \dot{z}_1 = -\lambda_2 sign(z_0 - \boldsymbol{\eta}_m(t)) \end{cases} \tag{21}$$

where $\lambda_1, \lambda_2 > 0$. z_0 and z_1 are auxiliary functions. $\hat{\boldsymbol{\eta}}_m(t)$ is the output of the differentiator. i.e., the estimate of $\dot{\boldsymbol{\eta}}_m(t)$. Moreover, the following saturation function $sat(.)$ is used instead of the $sign(.)$ function to avoid the chattering effect in the velocity estimation.

$$sat((z_0 - \boldsymbol{\eta}_m(t))/\varphi) = \begin{cases} 1, & (z_0 - \boldsymbol{\eta}_m(t)) > \varphi \\ (z_0 - \boldsymbol{\eta}_m(t))/\varphi, & |(z_0 - \boldsymbol{\eta}_m(t))/\varphi| \le 1 \\ -1, & (z_0 - \boldsymbol{\eta}_m(t)) < \varphi \end{cases} \tag{22}$$

where φ is the thickness of the boundary layer. φ is usually chosen as a very small positive value. The robust exact differentiator can be rewritten as follows:

$$\begin{cases} \dot{z}_0 = \hat{\boldsymbol{\eta}}_m(t) \\ \dot{z}_0 = -\lambda_1 |\dot{z}_0 - \boldsymbol{\eta}_m(t)|^{1/2} sat((z_0 - \boldsymbol{\eta}_m(t))/\varphi) + z_1 \\ \dot{z}_1 = -\lambda_2 sat((z_0 - \boldsymbol{\eta}_m(t))/\varphi) \end{cases} \tag{23}$$

Thus, we obtain the estimate $\hat{\dot{\boldsymbol{\eta}}}_m$, which is used in the control law (15).

Remark 5 It is worth noting that the RED does not need to be used in the proposed control law throughout the entire trace, only when the AUV arrives at the neighborhood of the target point. One reason is that we aim to improve the position precision of the target points while reducing the amount of computation. The other reason is that the parameters of RED are difficult to obtain.

Remark 6 The RED can be employed in real-time control systems and the use of the RED is preferable in high-precision systems with small noise [49].

3.4 The Target Points Tracking Algorithm

In this subsection, the proposed complete algorithm for the target points tracking is described in Algorithm 1. Note that the proposed algorithm requires little computing time, so it has high timeliness in real-time control. In addition, the proposed algorithm is suitable for tracking applications, where the acoustic underwater positioning has been implemented commercially [38].

Algorithm 1 The proposed complete algorithm for real time tracking

1: Set the initial parameters $\boldsymbol{v}(0)$,$\boldsymbol{\tau}(0)$, and $\boldsymbol{\eta}(0)$ to zero.
2: **while** $0 < d(t) < d_{max}$ **do**
3: Get the measurement position signal $\boldsymbol{\eta}_m(t - d(t))$ containing the noise from the GIB system, and obtain the corresponding position error $\boldsymbol{\eta}_d - \boldsymbol{\eta}_m(t - d(t))$.
4: Use the RED to obtain the estimated derivative of the position $\hat{\dot{\boldsymbol{\eta}}}_m(t - d(t))$.
5: Choose appropriate gain matrices $\boldsymbol{K}_P$ and $\boldsymbol{K}_D$.
6: Substitute the above parameters and measurement delay $d(t)$ into the presented control law equation (15).
7: **end while**

4 Simulation

In this section, simulations for the proposed controller are performed in MATLAB 2014a adopting a fourth-order Runge–Kutta approach with a fixed step size of 0.01 s. For simplicity, $\psi(t) = \psi_c = 0$ and $r(t) = 0$. Thus, the motion in yaw is not considered. The AUV hydrodynamic parameters utilized from Kim et al. [28] are presented in Table 1, where the $k_{\min}$ is equal to 16 kg/s. The target point positions of tracking tasks are presented as: $\boldsymbol{P}_A = [55, 70, -60]^T$ m, $\boldsymbol{P}_B = [55, 50, -60]^T$ m, $\boldsymbol{P}_C = [35, 50, -60]^T$ m, $\boldsymbol{P}_D = [35, 70, -60]^T$ m and the starting location of the AUV is $\boldsymbol{P}_S = [70, 80, 0]^T$ m on the surface, with an initial position error. The target points have the same constant depth −60 m. This research can be applied to seabed surveys. The simulation process time is 125 s and the target point change time is 25 s ($\boldsymbol{P}_S \rightarrow \boldsymbol{P}_A \rightarrow \boldsymbol{P}_B \rightarrow \boldsymbol{P}_C \rightarrow \boldsymbol{P}_D \rightarrow \boldsymbol{P}_A$). The linear/quadratic damping coefficients are set to vary by 20% from their true values in the AUV model. In particular, when AUV tracks target points $\boldsymbol{P}_A$ and $\boldsymbol{P}_C$, the coefficients increase by 20%, and when AUV tracks target points $\boldsymbol{P}_B$ and $\boldsymbol{P}_D$, the coefficients decrease by 20%. The control variables are given as $\boldsymbol{K}_P = \text{diag}\{25, 22, 12\}$ and $\boldsymbol{K}_D = \text{diag}\{-58, -55, -45\}$, which are obtained heuristically. First, $\boldsymbol{K}_P$ is chosen, taking into account the positions of target points. Based on the simulation results, $\boldsymbol{K}_P$ is adjusted to improve the tracking accuracy for target points. Second, fixing $\boldsymbol{K}_P$, $\boldsymbol{K}_D$ is adjusted to improve the tracking accuracy based on the simulation results.

We use the LMI-optimization toolbox of MATLAB to obtain the allowable measurement delay upper bound $d_{\max} = 0.723$ s. The allowable measurement delay lower bound $d_{\min}$ is 0 s.

4.1 The Proposed Controller Utilizing Different Measurement Delays

For this trial, the measurement noise is not considered. The proposed controller utilizing different measurement delays is tested for AUV under system uncertainties.

4.1.1 The Proposed Controller Utilizing an Allowable Time-varying Measurement Delay

According to the lower and upper bounds of the measurement delay, the allowable time-varying measurement delay can be set to $d(t) = 0.723\sin(t)$ s. The $\dot{d}(t) = 0.723\cos(t)$ also has lower and upper bounds.

The buoys in the GIB system are deployed on the surface and are fixed. The range of motion of the AUV is in an area of $80 \times 100 \times 80\text{m}^3$ where the maximum distance between the buoy and an arbitrary AUV is approximately 151 m. The speed of sound propagation in water is approximately 1500 m/s. Here, $d(t) = d_{ca}(t) + d_{co}(t)$. The calculated time $d_{ca}(t)$ is set to be very small and much less than $d_{co}(t)$, i.e., $0 < d_{ca}(t) \ll d_{co}(t)$, such that $1500\text{m/s} \times (0.723\text{s} - d_{ca}(t)) > 151\text{m}$. This shows that the measurement delay is allowable when AUV performs the

tasks in the area of $80 \times 100 \times 80\text{m}^3$. A longer distance between the AUV and buoys generally corresponds to greater measurement delay. For simplicity, we ignore the relationship between distance and measurement delay. Our main focus shifts to the target points ($\boldsymbol{P}_A$, $\boldsymbol{P}_B$, $\boldsymbol{P}_C$, and $\boldsymbol{P}_D$) tracking of the AUV under the given measurement delay $d(t) = 0.723\sin(t)$ s. Figure 5 presents the position trajectory of the proposed controller utilizing the allowable measurement delay $d(t) = 0.723\sin(t)$. This indicates that the target point tracking task is achieved using our proposed controller with allowable measurement delay.

4.1.2 The Proposed Controller Utilizing a Non-allowable Measurement Delay

Here, all the initial conditions except for the calculation time d_{ca} are the same as in the previous simulation in Sect. 4.1.1. d_{ca} is set very large such that the measurement delay $d(t)$ is greater than 0.723 s. For simplicity, we assume that the measurement delay $d(t)$ is always equal to 1 s when the AUV travels in the area of $80 \times 100 \times 80\text{m}^3$. Figure 6 describes the 3D position trajectory with the proposed controller utilizing a non-allowable measurement delay $d(t) = 1$ s. This figure shows that the positions of AUV cannot converge to the desired values of target points when the proposed controller uses the non-allowable measurement delay.

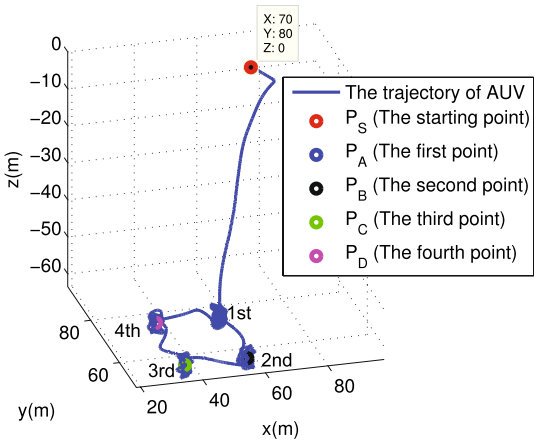

Fig. 6 AUV 3D position trajectory of the proposed controller utilizing the non-allowable measurement delay $d(t) = 1$ s

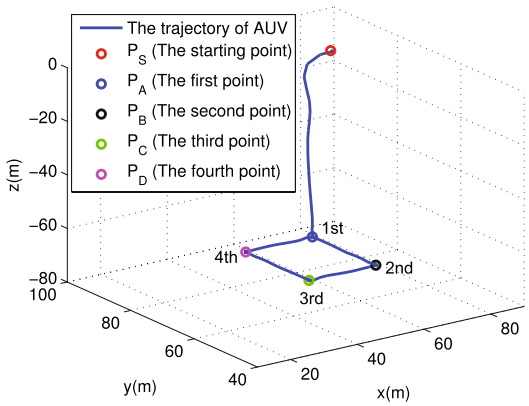

(a) 3D position trajectory

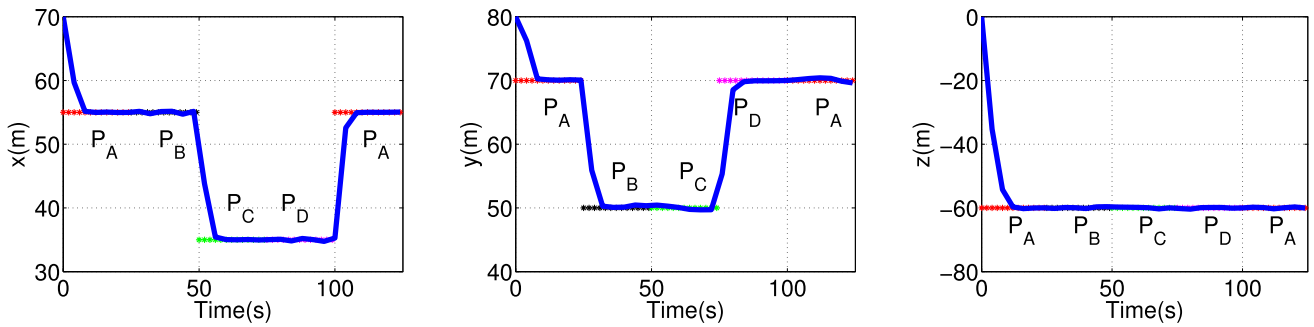

(b) Trajectory over time per projection plane

Fig. 5 AUV position trajectory of the proposed controller utilizing the allowable measurement delay $d(t) = 0.723\sin(t)$

4.2 The Proposed Controller Utilizing Robust Exact Differentiation against Numerical Differentiation Method

We consider the measurement noise and compare the proposed controller utilizing the RED with the proposed controller utilizing the traditional numerical differentiation method. When the AUV arrives at the neighborhood of a target point, the measurement signal $\boldsymbol{\eta}_m$ and its derivative both change very little. The Lipschitz's constant L_c can be set to 1. According to [49], we let $\lambda_1 = 1$ and $\lambda_2 = 1.1$. φ is set to 0.003. The measurement noise $\boldsymbol{\zeta}(t)$ is a Gaussian white noise with zero mean and variance 4×10^{-4}m. Then, the root-mean-square (RMS) errors at steady state for $\boldsymbol{P}_A$(15 s to 25 s), $\boldsymbol{P}_B$ (40 s to 50 s), $\boldsymbol{P}_C$ (65 s to 75 s), and $\boldsymbol{P}_D$ (90 s to 100 s) are calculated and presented in Table 2. The results show that the proposed controller utilizing the RED offers better tracking accuracy in the positions of target points than the proposed controller utilizing the traditional numerical differentiation method. We note that the proposed controller utilizing the RED outperforms the proposed controller utilizing the traditional numerical differentiation method in RMS error by approximately 61.2−79.1%. Moreover, Fig. 7 presents the control input of both controllers in all directions. It is clear that the proposed controller using the RED has a smaller control signal than the controller using the numerical differentiation method. It is shown that the proposed controller using the RED can effectively reduce the energy consumption of AUV, which increases the work time for AUV to perform deep sea tasks.

4.3 Evaluating Current Controllers under Measurement Delay and Measurement Noise

The proposed controller is challenged for $d(t) = 0.723\sin(t)$ s, against the conventional PD controller, and MPC controller. The new measurement noise $\boldsymbol{\zeta}(t)$ is a Gaussian white noise with zero mean and variance 2×10^{-4}m. The RED parameters are the same as those in the previous trial, while for a fair comparison, the control parameters of PD are the same as the proposed controller. For PD controller, the derivative of position signal is acquired by a traditional numerical differentiation method. Then, we compare the proposed controller with an advanced control strategy, i.e., the MPC. The parameters for MPC are presented in Table 1, while the type of MPC algorithm is a state feedback predictive control (SFPC) with the cost function defined as follows:

$$J(k) = \|Y(k) - Y_d(k)\|^2_{Q_c} + \| \triangle U(k)\|^2_{R_c} \tag{24}$$

where $\|x\|^2_A = x^T Ax$; $Y(k)$ and $Y_d(k)$ represent the predicted position and the desired position, respectively, Q_c and R_c are the weighting factors of the output and control signals, and $\triangle U(k)$ denotes the control input increment. Note that we apply the ZOH technique on MPC to bridge the domain difference between the system model and the control synthesis. Figure 8 describes the position tracking results, and Table 3 illustrates the RMS errors at steady state for various controllers. These results indicate that the PD controller under the measurement delay and measurement noise affords a mediocre positional accuracy. In contrast to the PD controller, both the MPC controller and the proposed controller precisely achieve the target point tracking. In particular, the proposed controller outperforms the conventional PD controller in RMS error by approximately 62.3−80.7%. Given that the suggested method meets the requirement of high tracking accuracy, we also examine the computational burden of each method. Table 4 presents the average calculation time of each controller in a single step, revealing that the proposed controller requires 89.7% less average calculation time than the MPC. Given the limited energy resources of an AUV, exploiting MPC controller poses a disadvantage for AUV applications.

These trials show that the proposed controller achieves excellent tracking performance with fewer RMS error while only a minor calculation time is required. Finally, it is important to note that during our trials, we challenge our proposed controller only against open-source controllers, namely the conventional PD, and MPC controllers, since re-implementing current controllers might lead to a non-optimized solution that would inevitably underestimate the capabilities of the original method.

5 Conclusion

In this paper, a new control method is presented for AUV target point tracking. The presented method considers measurement noise and measurement delay, and additionally, all

Table 2 RMS errors (m) at the steady state for the proposed controller using RED against numerical differentiation method under measurement noise $\boldsymbol{\zeta}(t)$ and measurement delay $d(t) = 0.723\sin(t)$ s

The proposed controller	RMS error ($\boldsymbol{P}_A$)			RMS error ($\boldsymbol{P}_B$)			RMS error ($\boldsymbol{P}_C$)			RMS error ($\boldsymbol{P}_D$)		
	Surge	Sway	Heave	Surge	Sway	Heave	Surge	Sway	Heave	Surge	Sway	Heave
Using the RED	0.082	0.041	0.026	0.079	0.039	0.025	0.082	0.040	0.028	0.076	0.039	0.027
Using the numerical differentiation	0.229	0.173	0.117	0.221	0.169	0.114	0.231	0.171	0.131	0.196	0.170	0.129

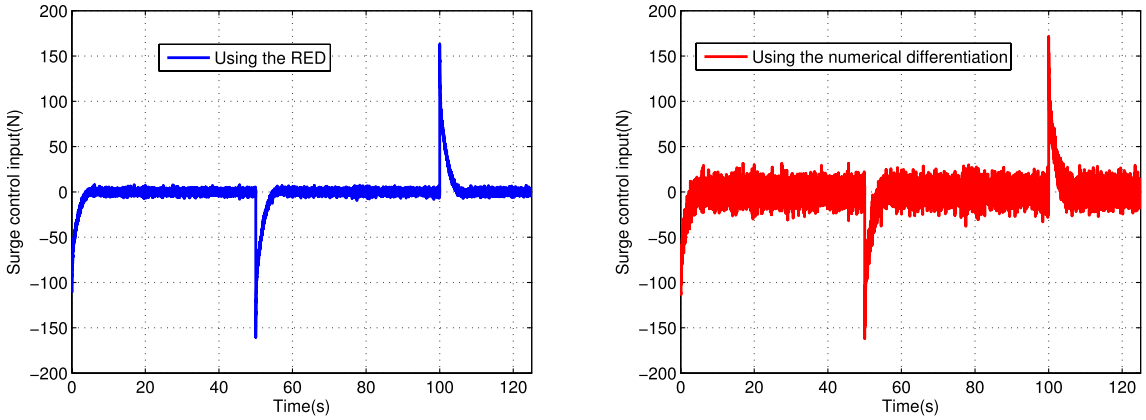

(a) Control input in surge

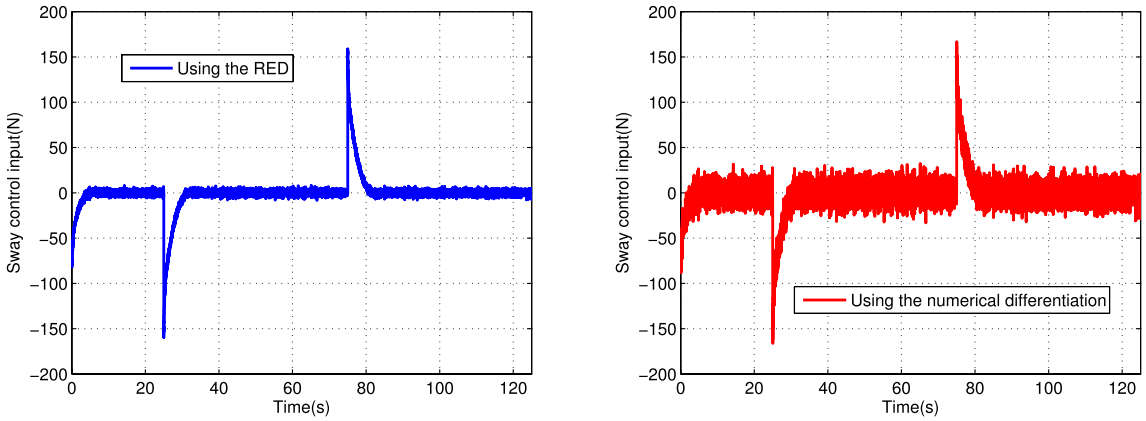

(b) Control input in sway

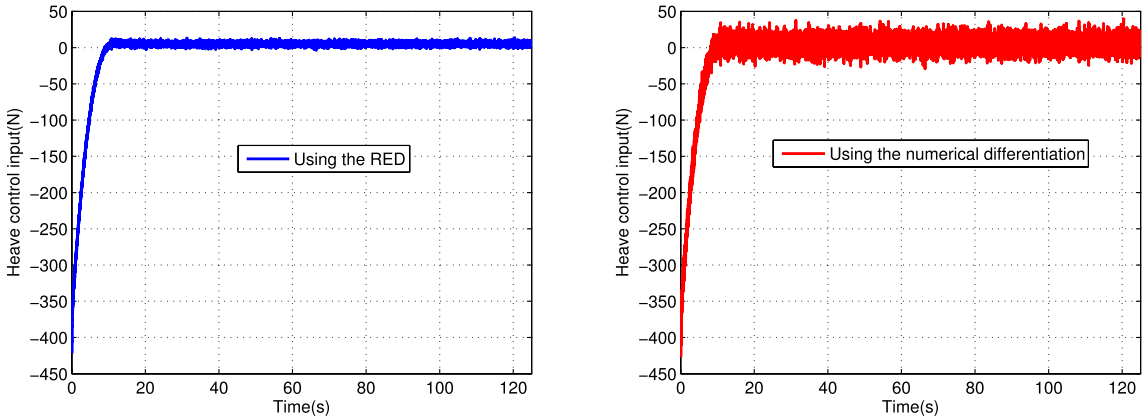

(c) Control input in heave

Fig. 7 The control input of proposed controller using RED against numerical differentiation method under measurement noise $\boldsymbol{\zeta}(t)$ and measurement delay $d(t) = 0.723\sin(t)$ s

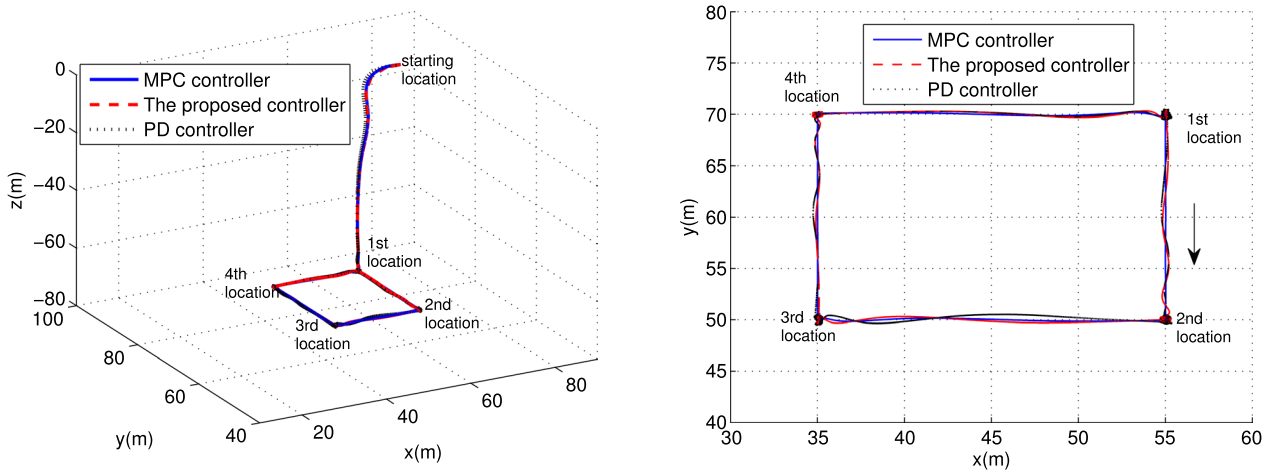

(a) 3D position trajectory (b) the path of target points for various controllers

Fig. 8 AUV position trajectory for MPC controller [26], PD controller, and the proposed controller under measurement delay 0.723 sin(t) s and measurement noise $\boldsymbol{\zeta}(t)$

Table 3 RMS errors (m) at the steady state for various controllers under measurement noise $\boldsymbol{\zeta}(t)$ and measurement delay 0.723 sin(t) s

Controller	RMS error ($\boldsymbol{P}_A$)			RMS error ($\boldsymbol{P}_B$)			RMS error ($\boldsymbol{P}_C$)			RMS error ($\boldsymbol{P}_D$)		
	Surge	Sway	Heave	Surge	Sway	Heave	Surge	Sway	Heave	Surge	Sway	Heave
PD controller	0.217	0.168	0.112	0.220	0.166	0.109	0.227	0.170	0.128	0.191	0.165	0.122
The proposed controller	0.079	0.038	0.027	0.077	0.032	0.026	0.078	0.038	0.029	0.081	0.039	0.027
MPC controller [26]	0.052	0.031	0.019	0.050	0.030	0.018	0.053	0.032	0.026	0.051	0.029	0.019

the hydrodynamic parameters to be unknown, which is the norm for practical applications. The suggested controller with appropriate control gains and measurement delay can achieve high steady-state tracking accuracy. The simulation results demonstrate the effectiveness of the proposed scheme. In particular, the proposedour controller outperforms the conventional time-delay controller in root-mean-square error by approximately 62.3−80.7%. Moreover, compared to the model predictive control, the proposedour controller requires 89.7% less average calculation time. Thus, the proposed controller has two advantages, i.e., high tracking accuracy and appealing computational complexity. In addition, by comparing the control input of the proposed controller utilizing robust exact differentiation against the numerical differentiation method, it can be found that the proposed controller utilizing robust exact differentiation can effectively reduce the energy consumption of AUV, which increases the work time for AUV to perform deep sea tasks. However, the method presented in this work has some limitations. First, the proposed controller does not consider the performance indicator of error convergence speed. The finite-time convergence for target points needs to be studied. Second, the method is limited to target point tracking. Therefore, it should be extended to path tracking for future research.

Table 4 The average calculation time of each controller in single step (measurement noise $\boldsymbol{\zeta}(t)$ and measurement delay 0.723 sin(t) s)

Controller	Time(ms)
The PD controller	0.041
The proposed controller	0.091
The MPC controller [26]	0.883

Appendix A The notations for Theorem 1

$$\Phi_{1,k}(\eta,\dot{\eta}) = \hat{\boldsymbol{S}} + \hat{\boldsymbol{R}} + \hat{\boldsymbol{F}} + \hat{\boldsymbol{A}} + \hat{\boldsymbol{H}} + \hat{\boldsymbol{K}} + \hat{\boldsymbol{E}} + \hat{\boldsymbol{B}} + \hat{\boldsymbol{G}},$$

$$\Gamma = [\boldsymbol{G}_0^T \quad \boldsymbol{G}_1^T \quad \boldsymbol{G}_2^T \quad \boldsymbol{G}_3^T],$$

$$\boldsymbol{G}_0^T = [\boldsymbol{0}_3 \quad \boldsymbol{0}_3 \quad \boldsymbol{0}_3 \quad \boldsymbol{0}_3 \quad \boldsymbol{I}_3 \quad \boldsymbol{0}_3 \quad \boldsymbol{0}_3 \quad \boldsymbol{0}_3 \quad \boldsymbol{0}_3],$$

$$\boldsymbol{G}_1^T = [\boldsymbol{0}_3 \quad \boldsymbol{0}_3 \quad \boldsymbol{0}_3 \quad \boldsymbol{I}_3 \quad \boldsymbol{0}_3 \quad \boldsymbol{I}_3 - 2\boldsymbol{I}_3 \quad \boldsymbol{0}_3 \quad \boldsymbol{0}_3],$$

$$\boldsymbol{G}_2^T = [\boldsymbol{0}_3 \quad \boldsymbol{0}_3 \quad \boldsymbol{0}_3 \quad \boldsymbol{0}_3 \quad \boldsymbol{I}_3 \quad \boldsymbol{0}_3 \quad \boldsymbol{0}_3 \quad \boldsymbol{0}_3 \quad \boldsymbol{I}_3],$$

$$\boldsymbol{G}_3^T = [\boldsymbol{0}_3 \quad \boldsymbol{I}_3 \quad \boldsymbol{0}_3 \quad \boldsymbol{0}_3 \quad \boldsymbol{0}_3 \quad \boldsymbol{I}_3 \quad \boldsymbol{0}_3 \quad -2\boldsymbol{I}_3 \quad \boldsymbol{0}_3],$$

$$\hat{\boldsymbol{R}} = \mathrm{diag}\{d_{\max}\boldsymbol{R}, \boldsymbol{0}_{24}\}, \ \tilde{\boldsymbol{R}} = \mathrm{diag}\{\boldsymbol{R}, 3\boldsymbol{R}\}$$

$$\hat{\boldsymbol{F}} = \mathrm{diag}\{\boldsymbol{F}, \boldsymbol{0}_3, -(1-\dot{d}(t))\boldsymbol{F}, \boldsymbol{0}_{18}\},$$

$$\hat{\boldsymbol{G}} = \mathrm{diag}\{\boldsymbol{0}_3, \boldsymbol{0}_3, \boldsymbol{0}_3, \boldsymbol{0}_3, -\boldsymbol{G}, \boldsymbol{0}_3, -\boldsymbol{G}, \boldsymbol{0}_3, \boldsymbol{0}_3\},$$

$$\hat{\boldsymbol{S}} = (\boldsymbol{S}_{i,j})_{9\times 9} \quad \text{with} \quad \boldsymbol{S}_{1,1} = -2k_{\min}\boldsymbol{I}_3,$$

$$\boldsymbol{S}_{1,2} = -\boldsymbol{K}_p, \quad \boldsymbol{S}_{1,3} = \boldsymbol{K}_D,$$

and the others are $\boldsymbol{0}_3$,

$$\hat{\boldsymbol{A}} = (\hat{\boldsymbol{A}}_{i,j})_{9\times 9} \quad \text{with} \quad \hat{\boldsymbol{A}}_{1,2} = \boldsymbol{A},$$

$$\hat{\boldsymbol{E}} = (\hat{\boldsymbol{E}}_{i,j})_{9\times 9} \quad \text{with} \quad \hat{\boldsymbol{E}}_{2,8} = d(t)\boldsymbol{E},$$

$$\hat{\boldsymbol{E}}_{6,8} = -d(t)[1-\dot{d}(t)\boldsymbol{E}]$$

and the others are $\boldsymbol{0}_3$,

$$\hat{\boldsymbol{B}} = (\hat{\boldsymbol{B}}_{i,j})_{9\times 9} \quad \text{with} \quad \hat{\boldsymbol{B}}_{4,7} = -(d_{\max} - d(t))\boldsymbol{B},$$

$$\hat{\boldsymbol{B}}_{6,7} = (d_{\max} - d(t))[1-\dot{d}(t)\boldsymbol{B}]$$

and the others are $\boldsymbol{0}_3$,

$$\hat{\boldsymbol{H}} = \boldsymbol{H}\boldsymbol{Z}_1, \hat{\boldsymbol{K}} = \boldsymbol{K}\boldsymbol{Z}_2 \quad \text{with}$$

$$\boldsymbol{Z}_1 = [\boldsymbol{0}_3 \quad 2\boldsymbol{I}_3 \quad \boldsymbol{0}_3 \quad \boldsymbol{0}_3 \quad \boldsymbol{0}_3 - 2\boldsymbol{I}_3 \quad \boldsymbol{0}_3 \quad \boldsymbol{0}_n - 2\boldsymbol{I}_3]$$

and

$$\boldsymbol{Z}_2 = [\boldsymbol{0}_3 \quad \boldsymbol{0}_3 \quad \boldsymbol{0}_3 - 2\boldsymbol{I}_3 - 2\boldsymbol{I}_3 - 2\boldsymbol{I}_3 \quad \boldsymbol{0}_3 \quad \boldsymbol{0}_3 \quad \boldsymbol{0}_3].$$

Appendix B The proof for Theorem 1 [43]

The Lyapunov functional candidate is given by

$$V = \sum_{i=1}^{6} V_i \tag{B1}$$

where

$$V_1 = \dot{\eta}^T \boldsymbol{M}_\eta \dot{\eta} \tag{B2}$$

$$V_2 = \boldsymbol{e}^T \boldsymbol{A} \boldsymbol{e} \tag{B3}$$

$$V_3 = \int_{t-d_{\max}}^{t-d(t)} \boldsymbol{e}^T(s)\boldsymbol{G}\boldsymbol{e}(s)\,ds \tag{B4}$$

$$V_4 = \int_{-d_{\max}}^{0}\int_{t+\sigma}^{t} \dot{\eta}^T(s)\boldsymbol{R}\dot{\eta}(s)\,ds d\sigma \tag{B5}$$

$$V_5 = \int_{t-d(t)}^{t} \boldsymbol{e}^T(s)\,ds \boldsymbol{E} \int_{t-d(t)}^{t} \boldsymbol{e}(s)\,ds + \int_{t-d_{\max}}^{t-d(t)} \boldsymbol{e}^T(\sigma)\,d\sigma \boldsymbol{B} \int_{t-d_{\max}}^{t-d(t)} \boldsymbol{e}(\sigma)\,d\sigma \tag{B6}$$

$$V_6 = \int_{t-d(t)}^{t} \dot{\eta}^T(s)\boldsymbol{F}\dot{\eta}(s)\,ds \tag{B7}$$

The given functional equation (B1) is positive definite since $\boldsymbol{M}_\eta \succ 0$, $\boldsymbol{R} \succ 0$, $\boldsymbol{F} \succ 0$, $\boldsymbol{A} \succ 0$, $\boldsymbol{G} \succ 0$, $\boldsymbol{E} \succ 0$, and $\boldsymbol{B} \succ 0$. Differentiating V_1, we obtain

$$\dot{V}_1 = \ddot{\eta}^T \boldsymbol{M}_\eta \dot{\eta} + \dot{\eta}^T \dot{\boldsymbol{M}}_\eta \dot{\eta} + \dot{\eta}^T \boldsymbol{M}_\eta \ddot{\eta} \tag{B8}$$

From $\boldsymbol{M}_\eta^T = \boldsymbol{M}_\eta$, $\boldsymbol{M}_\eta\ddot{\eta} = \boldsymbol{\tau}_\eta - \boldsymbol{C}_\eta\dot{\eta} - \boldsymbol{D}_\eta\dot{\eta} - \boldsymbol{g}_\eta$, and $\boldsymbol{\tau}_\eta^T\dot{\eta} = \{\boldsymbol{\tau}_\eta^T\dot{\eta}\}^T = \dot{\eta}^T\boldsymbol{\tau}_\eta$, one yields

$$\dot{V}_1 = 2\dot{\eta}^T\boldsymbol{\tau}_\eta - 2\dot{\eta}^T\boldsymbol{g}_\eta - 2\dot{\eta}^T\boldsymbol{D}_\eta\dot{\eta} - 2\dot{\eta}^T\boldsymbol{C}_\eta\dot{\eta} + \dot{\eta}^T\dot{\boldsymbol{M}}_\eta\dot{\eta} \tag{B9}$$

Using the skew-symmetric property $s^T(\dot{\boldsymbol{M}}_\eta - 2\boldsymbol{C}_\eta)s = 0$, we obtain

$$\dot{V}_1 = 2\dot{\eta}^T\boldsymbol{\tau}_\eta - 2\dot{\eta}^T\boldsymbol{g}_\eta - 2\dot{\eta}^T\boldsymbol{D}_\eta\dot{\eta} \tag{B10}$$

In this paper, we consider 3-DOF motions and obtain

$$\boldsymbol{D}(v) = \mathrm{diag}\{k_u, k_v, k_w\} + \mathrm{diag}\{k_{u|u|}|u(t)|, k_{v|v|}|v(t)|, k_{w|w|}|w(t)|\} \tag{B11}$$

Then let $\boldsymbol{D}(v) = \boldsymbol{D}_1 + \boldsymbol{D}_2|\boldsymbol{v(t)}|$ with $\boldsymbol{D}_1 = \mathrm{diag}\{k_u, k_v, k_w\}$ and $\boldsymbol{D}_2 = \mathrm{diag}\{k_{u|u|}, k_{v|v|}, k_{w|w|}\}$. Because $\boldsymbol{J}^{-T}\boldsymbol{D}_1\boldsymbol{J}^{-1}$ and $\boldsymbol{D}_1$ have the same eigenvalues, we obtain

$$-\dot{\eta}^T\boldsymbol{D}_\eta\dot{\eta} < -\dot{\eta}^T\boldsymbol{J}^{-T}\boldsymbol{D}_1\boldsymbol{J}^{-1}\dot{\eta} < -\dot{\eta}^T\boldsymbol{D}_{\min}\dot{\eta} \tag{B12}$$

where $\boldsymbol{D}_{\min} = \mathrm{diag}\{k_{\min}, k_{\min}, k_{\min}\}$ and $k_{\min} = min\{k_u, k_v, k_w\}$. Then we obtain

$$\dot{V}_1 < 2\dot{\eta}^T\boldsymbol{\tau}_\eta - 2\dot{\eta}^T\boldsymbol{g}_{\boldsymbol{\eta}} - 2\dot{\eta}^T\boldsymbol{D}_{\min}\dot{\eta} \tag{B13}$$

We use the control law (15) and Newton Leibniz formula, and obtain

$$\dot{V}_1 < -2\dot{\eta}^T\boldsymbol{K}_P(-\int_{t-d(t)}^{t}\dot{\eta}(s)ds + \boldsymbol{e}) + 2\dot{\eta}^T\boldsymbol{K}_D\dot{\eta}(t-d(t)) - 2\dot{\eta}^T\boldsymbol{D}_{\min}\dot{\eta} \tag{B14}$$

The time derivative of V_2 is

$$\dot{V}_2 = \boldsymbol{e}^T(\boldsymbol{A} + \boldsymbol{A}^T)\dot{\boldsymbol{e}} \tag{B15}$$

Differentiating V_3, we obtain

$$\dot{V}_3 = \boldsymbol{e}^T(t-d(t))\boldsymbol{G}\boldsymbol{e}(t-d(t))(1-\dot{d}(t)) - \boldsymbol{e}^T(t-d_{\max})\boldsymbol{G}\boldsymbol{e}(t-d_{\max}) \tag{B16}$$

The time derivative of V_4 is

$$\dot{V}_4 = d_{\max}\dot{\eta}^T\boldsymbol{R}\dot{\eta} - \int_{t-d_{\max}}^{t}\dot{\eta}^T(s)\boldsymbol{R}\dot{\eta}(s)ds \tag{B17}$$

Splitting the integral $[t-d_{\max}, t]$ into two integrals $[t-d_{\max}, t-d(t)]$ and $[t-d(t), t]$, we obtain

$$\dot{V}_4 = d_{\max}\dot{\eta}^T\boldsymbol{R}\dot{\eta} - \int_{t-d_{\max}}^{t-d(t)}\dot{\eta}^T(s)\boldsymbol{R}\dot{\eta}(s)ds - \int_{t-d(t)}^{t}\dot{\eta}^T(s)\boldsymbol{R}\dot{\eta}(s)ds \tag{B18}$$

We employ Lemma 1, obtaining

$$-\int_{t-d_{\max}}^{t-d(t)}\dot{\eta}^T(s)\boldsymbol{R}\dot{\eta}(s)ds = \frac{1}{d_{\max}-d(t)}\xi^T\boldsymbol{W}_{01}^T\begin{bmatrix}\boldsymbol{R} & \boldsymbol{0}_n\\ \boldsymbol{0}_n & 3\boldsymbol{R}\end{bmatrix}\boldsymbol{W}_{01}\xi \tag{B19}$$

and

$$-\int_{t-d(t)}^{t}\dot{\eta}^T(s)\boldsymbol{R}\dot{\eta}(s)ds \le -\frac{1}{d(t)}\xi^T\boldsymbol{W}_{23}^T\begin{bmatrix}\boldsymbol{R} & \boldsymbol{0}_n\\ \boldsymbol{0}_n & 3\boldsymbol{R}\end{bmatrix}\boldsymbol{W}_{23}\xi \tag{B20}$$

where $\boldsymbol{W}_{01} = [\boldsymbol{G}_0, \boldsymbol{G}_1]^T$ and $\boldsymbol{W}_{23} = [\boldsymbol{G}_2, \boldsymbol{G}_3]^T$. Then we get

$$-\int_{t-d_{\max}}^{t}\dot{\eta}^T(s)\boldsymbol{R}\dot{\eta}(s)ds \le -\xi^T\Big(\frac{1}{d_{\max}-d(t)}\boldsymbol{W}_{01}^T\begin{bmatrix}\boldsymbol{R} & \boldsymbol{0}_n\\ \boldsymbol{0}_n & 3\boldsymbol{R}\end{bmatrix}\boldsymbol{W}_{01} + \frac{1}{d(t)}\boldsymbol{W}_{23}^T\begin{bmatrix}\boldsymbol{R} & \boldsymbol{0}_n\\ \boldsymbol{0}_n & 3\boldsymbol{R}\end{bmatrix}\boldsymbol{W}_{23}\Big)\xi \tag{B21}$$

We employ Lemma 2 and obtain

$$-\int_{t-d_{\max}}^{t}\dot{\eta}^T(s)\boldsymbol{R}\dot{\eta}(s)ds \le -\frac{1}{d_{\max}}\xi^T\Gamma^T\Phi_2\Gamma\xi \tag{B22}$$

Thus, we obtain

$$\dot{V}_4 \le d_{\max}\dot{\eta}^T\boldsymbol{R}\dot{\eta} - \frac{1}{d_{\max}}\xi^T\Gamma^T\Phi_2\Gamma\xi \tag{B23}$$

The time derivative of V_5 is

$$\dot{V}_5 = \int_{t-d(t)}^{t}\boldsymbol{e}^T(s)ds(\boldsymbol{E}+\boldsymbol{E}^T)\times\big(\boldsymbol{e}(t)-\boldsymbol{e}(t-d(t))(1-\dot{d}(t))\big) + \int_{t-d_{\max}}^{t-d(t)}\boldsymbol{e}^T(s)ds(\boldsymbol{B}+\boldsymbol{B}^T)\times\big(\boldsymbol{e}(t-d(t))(1-\dot{d}(t))-\boldsymbol{e}(t-d_{\max})\big) \tag{B24}$$

Differentiating V_6, we obtain

$$\dot{V}_6 = \dot{\eta}^T(t)\boldsymbol{F}\dot{\eta}(t) - \dot{\eta}^T(t-d(t))\boldsymbol{F}\dot{\eta}(t-d(t))(1-\dot{d}(t)) \tag{B25}$$

Auxiliary functions are constructed as follows:

$$f_1 = 0 = 2\xi^T\boldsymbol{H}[e(t)-e(t-d(t)) - \int_{t-d(t)}^{t}\dot{\eta}(s)ds] \tag{B26}$$

$$f_2 = 0 = 2\xi^T\boldsymbol{K}[e(t-d(t)) - e(t-d_{\max}) - \int_{t-d_{\max}}^{t-d(t)}\dot{\eta}(s)ds] \tag{B27}$$

Finally, we obtain

$$\dot{V} = \sum_{i=1}^{6}\dot{V}_i + \sum_{j=1}^{2}f_j \le \xi^T\Phi_1(\eta,\dot{\eta})\xi \tag{B28}$$

where

$\xi = [\dot{\eta}, \boldsymbol{e}, \dot{\eta}(t-d(t)), \boldsymbol{e}(t-d_{\max}), \int_{t-d_{\max}}^{t-d(t)}\dot{\eta}(s)ds, \boldsymbol{e}(t-d(t)), (\frac{1}{d_{\max}}-d(t))\int_{t-d_{\max}}^{t-d(t)}\boldsymbol{e}(s)ds, \frac{1}{d(t)}\int_{t-d(t)}^{t}\boldsymbol{e}(s)ds, \int_{t-d(t)}^{t}\dot{\eta}(s)ds]^T$ and $\Phi_1(\eta,\dot{\eta}) = \Phi_{1,k}(\eta,\dot{\eta}) - \frac{1}{d_{\max}}\Gamma^T\Phi_2\Gamma$.

If $\Phi_1(\eta,\dot{\eta}) \prec 0$, we can conclude that $\dot{V}$ is negative definite. The matrix $\Phi_1(\eta,\dot{\eta})$ is convex with respect to $d(t)$ and $\dot{d}(t)$. Therefore, it is sufficient to ensure that $\Phi_1 \prec 0$ at the vertices of the internals $[d_{\min}, d_{\max}] \times [a_{\min}, a_{\max}]$. Since V is positive definite, the AUV tracking system for a target point is asymptotically stable. This completes the proof.

Acknowledgements Not applicable.

Author Contributions Conceptualization: QL; methodology: QL; software: QL; writing original draft: QL; writing–review and editing: ML.

Funding The author(s) received no financial support for the research, authorship, and/or publication of this article.

Availability of data and materials The data presented in this study are available on request from the corresponding author.

Declarations

Conflict of interest The authors declare no conflict of interest.

Ethics approval and consent to participate All the authors have agreed to participate in this article.

Consent for publication All the authors approve the submission to this journal.

References

1. Fossen, T.I.: Guidance and control of ocean vehicles. University of Trondheim, Norway. Wiley, Chichester, England. ISBN: 0 471 94113 1, Doctors Thesis (1999)
2. Borlaug, I.-L.G., Pettersen, K.Y., Gravdahl, J.T.: Comparison of two second-order sliding mode control algorithms for an articulated intervention auv: Theory and experimental results. Ocean Eng. **222**, 108480 (2021)
3. Chen, M., Jiang, B., Zou, J., Feng, X.: Robust adaptive tracking control of the underwater robot with input nonlinearity using neural networks. Int. J. Comput. Intell. Syst. **3**(5), 646–655 (2010)
4. Cui, R., Ge, S.S., How, B.V.E., Choo, Y.S.: Leader-follower formation control of underactuated autonomous underwater vehicles. Ocean Eng. **37**(17–18), 1491–1502 (2010)
5. Zhan, D., Zheng, H., Xu, W.: Tracking control of autonomous underwater vehicles with acoustic localization and extended kalman filter. Appl. Sci. **11**(17), 8038 (2021)
6. Allotta, B., Caiti, A., Costanzi, R., Fanelli, F., Fenucci, D., Meli, E., Ridolfi, A.: A new auv navigation system exploiting unscented kalman filter. Ocean Eng. **113**, 121–132 (2016)
7. Paull, L., Saeedi, S., Seto, M., Li, H.: Auv navigation and localization: A review. IEEE J. Oceanic Eng. **39**(1), 131–149 (2013)
8. Ma, H., Mu, X., He, B.: Adaptive navigation algorithm with deep learning for autonomous underwater vehicle. Sensors **21**(19), 6406 (2021)
9. Saksvik, I. B., Alcocer, A., Hassani, V.: A deep learning approach to dead-reckoning navigation for autonomous underwater vehicles with limited sensor payloads. In: OCEANS 2021: San Diego–Porto, pp. 1–9 . IEEE (2021)
10. Yang, W., Fan, S., Xu, S., King, P., Kang, B., Kim, E.: Autonomous underwater vehicle navigation using sonar image matching based on convolutional neural network. IFAC-PapersOnLine **52**(21), 156–162 (2019)
11. Liu, T., Hu, Y., Xu, H.: Deep reinforcement learning for vectored thruster autonomous underwater vehicle control. Complexity **2021** 1–25 (2021)
12. Li, Z., Luo, X.: Autonomous underwater vehicles (auvs) path planning based on deep reinforcement learning. In: 2021 11th International Conference on Intelligent Control and Information Processing (ICICIP), pp. 125–129 . IEEE (2021)
13. Jalving, B.: The ndre-auv flight control system. IEEE J. Oceanic Eng. **19**(4), 497–501 (1994)
14. Li, J.-H., Lee, P.-M.: Design of an adaptive nonlinear controller for depth control of an autonomous underwater vehicle. Ocean Eng. **32**(17–18), 2165–2181 (2005)
15. Khalil, H.K.: Nonlinear systems third edition. Patience Hall **115** (2002)
16. Repoulias, F., Papadopoulos, E.: Planar trajectory planning and tracking control design for underactuated auvs. Ocean Eng. **34**(11–12), 1650–1667 (2007)
17. Liang, X., Qu, X., Hou, Y., Zhang, J.: Three-dimensional path following control of underactuated autonomous underwater vehicle based on damping backstepping. Int. J. Adv. Rob. Syst. **14**(4), 1729881417724179 (2017)
18. Xu, J., Wang, M., Qiao, L.: Dynamical sliding mode control for the trajectory tracking of underactuated unmanned underwater vehicles. Ocean Eng. **105**, 54–63 (2015)
19. Karkoub, M., Wu, H.-M., Hwang, C.-L.: Nonlinear trajectory-tracking control of an autonomous underwater vehicle. Ocean Eng. **145**, 188–198 (2017)
20. Liang, X., Qu, X., Wan, L., Ma, Q.: Three-dimensional path following of an underactuated auv based on fuzzy backstepping sliding mode control. Int. J. Fuzzy Syst. **20**(2), 640–649 (2018)
21. Li, J., Du, J., Sun, Y., Lewis, F.L.: Robust adaptive trajectory tracking control of underactuated autonomous underwater vehicles with prescribed performance. Int. J. Robust Nonlinear Control **29**(14), 4629–4643 (2019)
22. Wang, J., Wang, C., Wei, Y., Zhang, C.: On the fuzzy-adaptive command filtered backstepping control of an underactuated autonomous underwater vehicle in the three-dimensional space. J. Mech. Sci. Technol. **33**(6), 2903–2914 (2019)
23. Elhaki, O., Shojaei, K.: Neural network-based target tracking control of underactuated autonomous underwater vehicles with a prescribed performance. Ocean Eng. **167**, 239–256 (2018)
24. Peng, Z., Wang, J., Han, Q.-L.: Path-following control of autonomous underwater vehicles subject to velocity and input constraints via neurodynamic optimization. IEEE Trans. Industr. Electron. **66**(11), 8724–8732 (2018)
25. Wang, J., Wang, C., Wei, Y., Zhang, C.: Three-dimensional path following of an underactuated auv based on neuro-adaptive command filtered backstepping control. IEEE Access **6**, 74355–74365 (2018)
26. Yan, Z., Gong, P., Zhang, W., Wu, W.: Model predictive control of autonomous underwater vehicles for trajectory tracking with external disturbances. Ocean Eng. **217**, 107884 (2020)
27. Kumar, R.P., Dasgupta, A., Kumar, C.: Robust trajectory control of underwater vehicles using time delay control law. Ocean Eng. **34**(5–6), 842–849 (2007)
28. Kim, J., Joe, H., Yu, S.-C., Lee, J.S., Kim, M.: Time-delay controller design for position control of autonomous underwater vehicle under disturbances. IEEE Trans. Industr. Electron. **63**(2), 1052–1061 (2015)
29. Cho, G.R., Li, J.-H., Park, D., Jung, J.H.: Robust trajectory tracking of autonomous underwater vehicles using back-stepping control and time delay estimation. Ocean Eng. **201**, 107131 (2020)
30. Mazare, M., Taghizadeh, M., Ghaf-Ghanbari, P.: Pitch actuator fault-tolerant control of wind turbines based on time delay control and disturbance observer. Ocean Eng. **238**, 109724 (2021)
31. Wang, Y., Gu, L., Xu, Y., Cao, X.: Practical tracking control of robot manipulators with continuous fractional-order nonsingular terminal sliding mode. IEEE Trans. Industr. Electron. **63**(10), 6194–6204 (2016)
32. Roy, S., Kar, I.N., Lee, J., Tsagarakis, N.G., Caldwell, D.G.: Adaptive-robust control of a class of el systems with parametric

variations using artificially delayed input and position feedback. IEEE Trans. Control Syst. Technol. **27**(2), 603–615 (2017)
33. Ridao, P., Carreras, M., Ribas, D., Sanz, P.J., Oliver, G.: Intervention auvs: the next challenge. Annu. Rev. Control. **40**, 227–241 (2015)
34. Shi, Y., Shen, C., Fang, H., Li, H.: Advanced control in marine mechatronic systems: A survey. IEEE/ASME Trans. Mechatron. **22**(3), 1121–1131 (2017)
35. Stutters, L., Liu, H., Tiltman, C., Brown, D.J.: Navigation technologies for autonomous underwater vehicles. IEEE Trans. Syst. Man Cybern. Part C (Applications and Reviews) **38**(4), 581–589 (2008)
36. Wu, Y., Ta, X., Xiao, R., Wei, Y., An, D., Li, D.: Survey of underwater robot positioning navigation. Appl. Ocean Res. **90**, 101845 (2019)
37. Sahoo, A., Dwivedy, S.K., Robi, P.: Advancements in the field of autonomous underwater vehicle. Ocean Eng. **181**, 145–160 (2019)
38. Alcocer, A., Oliveira, P., Pascoal, A.: Study and implementation of an ekf gib-based underwater positioning system. Control. Eng. Pract. **15**(6), 689–701 (2007)
39. Mukherjee, K., Kar, I., Bhatt, R.: Region tracking based control of an autonomous underwater vehicle with input delay. Ocean Eng. **99**, 107–114 (2015)
40. Yan, J., Guo, Z., Yang, X., Luo, X., Guan, X.: Finite-time tracking control of autonomous underwater vehicle without velocity measurements. IEEE Trans. Syst. Man Cybern. Syst. **52**, 6759–6773 (2021)
41. Wang, Q., Zhang, Y., Dong, C., Ni, M.: Robust trajectory tracking of unstable aircraft with measurement delay. Proc. Inst. Mech. Eng. Part I: J. Syst. Control Eng. **226**(9), 1220–1230 (2012)
42. Yan, J., Gao, J., Yang, X., Luo, X., Guan, X.: Tracking control of a remotely operated underwater vehicle with time delay and actuator saturation. Ocean Eng. **184**, 299–310 (2019)
43. Yan, J., Gao, J., Yang, X., Luo, X., Guan, X.: Position tracking control of remotely operated underwater vehicles with communication delay. IEEE Trans. Control Syst. Technol. **28**(6), 2506–2514 (2019)
44. Shen, C., Shi, Y., Buckham, B.: Trajectory tracking control of an autonomous underwater vehicle using lyapunov-based model predictive control. IEEE Trans. Industr. Electron. **65**(7), 5796–5805 (2017)
45. Patre, B., Londhe, P., Waghmare, L., Mohan, S.: Disturbance estimator based non-singular fast fuzzy terminal sliding mode control of an autonomous underwater vehicle. Ocean Eng. **159**, 372–387 (2018)
46. Caccia, M., Veruggio, G.: Guidance and control of a reconfigurable unmanned underwater vehicle. Control. Eng. Pract. **8**(1), 21–37 (2000)
47. Seuret, A., Gouaisbaut, F.: Wirtinger-based integral inequality: application to time-delay systems. Automatica **49**(9), 2860–2866 (2013)
48. Park, P., Ko, J.W., Jeong, C.: Reciprocally convex approach to stability of systems with time-varying delays. Automatica **47**(1), 235–238 (2011)
49. Levant, A.: Robust exact differentiation via sliding mode technique. Automatica **34**(3), 379–384 (1998)